J Mater Sci (2008) 43:4031–4041
DOI 10.1007/s10853-007-2332-0

REES RAWLINGS FESTSCHRIFT

Oxidation of SiC powders for the preparation of SiC/mullite/alumina nanocomposites

Jingyan He · Clive Brian Ponton

Received: 15 June 2007 / Accepted: 19 November 2007 / Published online: 3 April 2008

Abstract The oxidation behaviour of two types of SiC powder of differing particle size and morphology distribution has been studied in the present work; one submicron-sized and the other micron-sized. It has been observed that the onset-temperature for significant oxidation of the SiC powder of smaller particle size is much lower than that for the SiC powder of larger particle size; namely, about 760 °C as compared with about 950 °C. Furthermore, the rate and extent of oxidation of the former SiC powder is much higher than that of the latter SiC powder. Interestingly, however, the SiC powder of smaller particle size exhibits more controllable oxidation behaviour in the context of the preparation of SiC/mullite/alumina nanocomposites, i.e., in terms of the extent of oxidation, and hence the amount of silica formed as an encapsulating outer layer and the resulting core SiC particle size, than the SiC powder of larger particle size. The SiO_2 layer formed was amorphous when the SiC powders were oxidized below 1,200 °C, but crystalline in the form of cristobalite when they were oxidized above 1,200 °C. Since the presence of amorphous silica can accelerate the sintering of the nanocomposite, oxidation of the chosen SiC powder should thus take place below 1,200 °C.

J. He
Institute for Materials Research, University of Leeds, Leeds LS2 9JT, UK
e-mail: prejh@leeds.ac.uk

C. B. Ponton (✉)
Department of Metallurgy and Materials, University of Birmingham, Edgbaston, Birmingham B15 2TT, UK
e-mail: c.b.ponton@bham.ac.uk

Introduction

Silicon carbide (SiC) is a candidate material for high-temperature structural applications because of its good mechanical properties, as well as excellent corrosion and oxidation resistance. Although SiC powder is processed into dense SiC monoliths for use in various applications, it is also used as a reinforcing agent to fabricate ceramic composites. Since SiC or SiC-containing composites are intended for high-temperature applications, their oxidation behaviour is an important issue.

The oxidation behaviour of SiC can be divided into two oxidation modes: passive and active. Passive oxidation forms a coherent, dense SiO_2 layer on the surface, which suppresses further oxidation [1]. On the contrary, active oxidation forms gaseous SiO, which dissipates away from the surface, promoting further oxidation; hence, the oxidation becomes severe [2–4]. The temperature at which the oxidation mode changes, from passive to active, decreases with decreasing oxygen partial pressure. For most applications, the oxidation of SiC should be constrained within the passive oxidation regime [5].

In the study of SiC passive oxidation at elevated temperatures, it is generally believed that the oxidation of SiC is similar to the oxidation of silicon. The oxidation process is accomplished by the diffusion of oxygen molecules or ions through the oxide layer [3, 4, 6, 7]. Most studies on the oxidation of SiC have focussed on SiC films or on bulk materials. However, the oxidation of SiC powder is also an essential step in the fabrication of some SiC-containing composites. For example, Holz and Claussen [8] and Wu and Claussen [9] produced compacts of alumina, silica and SiC by the oxidation of aluminium and SiC powder compacts, followed by reaction sintering of the alumina and silica layers to form

mullite. This process resulted in dense mullite/SiC composites with high-strength and low-sintering shrinkage. In another report, Sakka et al. [10] used alumina and SiC powder mixtures to fabricate SiC/mullite/alumina nanocomposites following similar procedures. Nevertheless, neither of these studies attempted to systematically vary the degree of oxidation to change the composition of the composites.

In order to produce better composites, it is often necessary to optimize the amount of each phase present in the composites. For example, in SiC/mullite/alumina composites, where the mullite is the reaction product of alumina and silica, the amount of silica available for reaction is determined by the degree of surface oxidation of the SiC powder particles. Therefore, it is essential to determine the oxidation kinetics of the SiC in the mixed powder, so that control of the composition of the final composite is made possible.

In this study, the oxidation behaviour of SiC particles in SiC powders and in pressure-filtered samples of alumina-seeded boehmite/SiC compacts was studied. Experiments were conducted at elevated temperatures in both static and flowing air for different times in order to determine the degree of oxidation. These data were the basis for the oxidation treatments used to produce the appropriate amount of silica for the subsequent reaction-sintering of the SiC/mullite/alumina composite material. The oxidation behaviour of the SiC samples subjected to different thermal cycles for different time periods was characterized using DTA, TGA and XRD techniques. Particle morphologies and sizes were evaluated using SEM, TEM and Laser diffraction particle size analysis.

Experimental procedure

Two types of α-SiC powder were used. One was polishing grade SiC (Electro Minerals Company Ltd, UK; denoted hereafter as P-SiC) with a mean particle diameter of 4.7 μm. The other one was ultrafine SiC (Grade UF45, H.C. Starck, Goslar, Germany; denoted hereafter as UF-SiC) with a mean particle size of 0.2 μm.

To study the oxidation of SiC particles within the SiC powders, the two types of SiC powder were loosely laid into alumina crucibles and spread to a depth of about 4 mm. The crucibles containing those powders were then heated in a furnace to temperatures in the range from 800 to 1,400 °C for different time periods ranging from 2 to 14 h at a heating/cooling rate of 10 °C/min, under both static and flowing air (flow rate of 30 cm^3/min, 1 bar pressure) conditions. The masses of the SiC powder samples before oxidation and changes in mass with oxidation were measured.

To calculate the mass fraction of SiC oxidized, f, the following equation has been derived (See Appendix A)

$$f = C_M/0.5 \quad (1)$$

where C_M is the relative mass change after oxidation.

For studying the oxidation of SiC particles in pressure-filtered compacts of alumina seeded boehmite/SiC composite material, a compact composition of 5 wt.% alumina seed content on the basis of total alumina content (alumina seeds plus alumina converted from boehmite) and 20 wt.% UF-SiC content based on the total amount of material (i.e., alumina seed plus boehmite and SiC) was used. For convenience, the compacts are denoted hereafter as BA_5/20 wt.% SiC.

Results and discussion

Effect of temperature and time on the oxidation of SiC

The TGA–DTA (Thermo Gravimetric Analysis–Differential Thermal Analysis) curves of the UF-SiC and P-SiC powders are shown in Figs. 1 and 2, respectively. From the DTA curve, the onset-temperature for significant oxidation of UF-SiC is about 760 °C, which is much lower than that for P-SiC, which is at about 950 °C; as evidenced by the first plateau and only plateau, respectively, in the DTA curves. This is because UF-SiC is much more reactive than P-SiC due to its much smaller particle size, and hence large surface area to volume ratio.

Figures 3 and 4 compare the effect of oxidation temperature for a holding time of 4 h and the effect of holding time at an oxidation temperature of 1,200 °C, respectively, on the relative mass change and mass fraction oxidized of the two SiC powders in static air. These data corroborate the onset-temperatures for significant oxidation determined from the TGA–DTA curves.

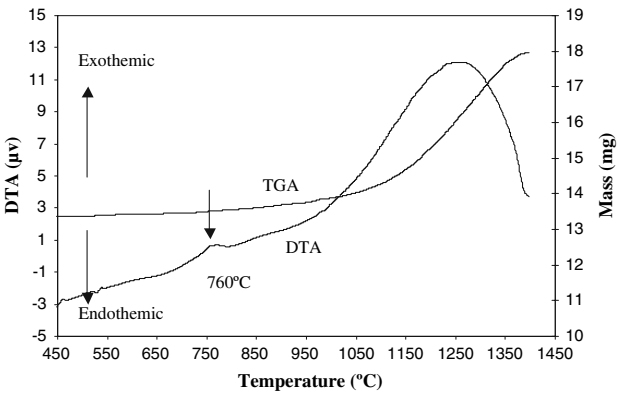

Fig. 1 TGA–DTA traces for UF-SiC

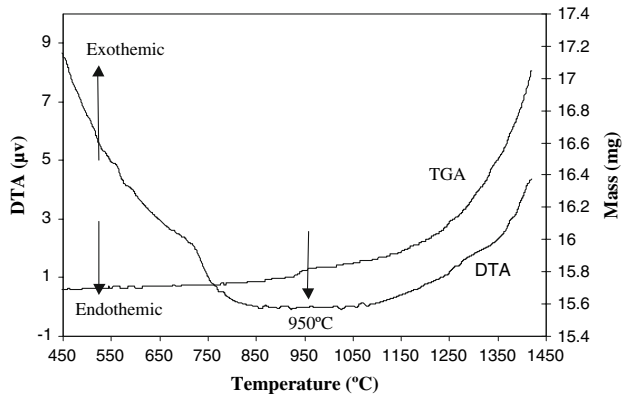

Fig. 2 TGA–DTA traces for P-SiC

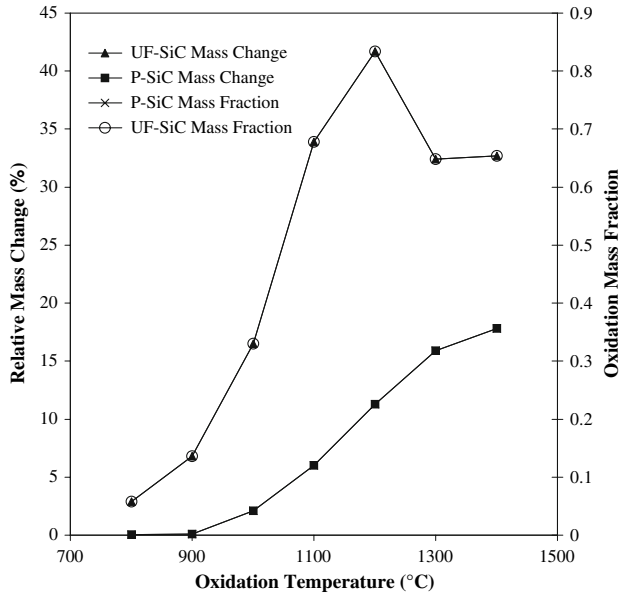

Fig. 3 Relative mass change and mass fraction oxidized against oxidation temperature (for 4 h oxidation time)

It is clear, on balance, and as expected, that the mass fraction oxidized increases as the oxidation temperature and/or holding time increases; yet, there are nonetheless distinct differences between the oxidation behaviour of P-SiC and UF-SiC. For P-SiC, the mass fraction oxidized increased with both oxidation temperature above 900 °C (being essentially zero at 900 °C) and time, although the maximum oxidation mass fraction was <0.4 under the experimental conditions used. In contrast, the mass fraction of UF-SiC oxidized at 900 °C was already 0.14, having started oxidising at about 800 °C, with the extent of oxidation increasing rapidly with temperature. At 1,200 °C, the oxidation of UF-SiC is very fast, so that after only a 2-h holding time, the oxidation mass fraction was 0.8. Above 1,200 °C, however, the mass fraction oxidized decreased to about 0.65. This could, in the case of the SiC-containing nanocomposite (see later), be due to reaction sintering

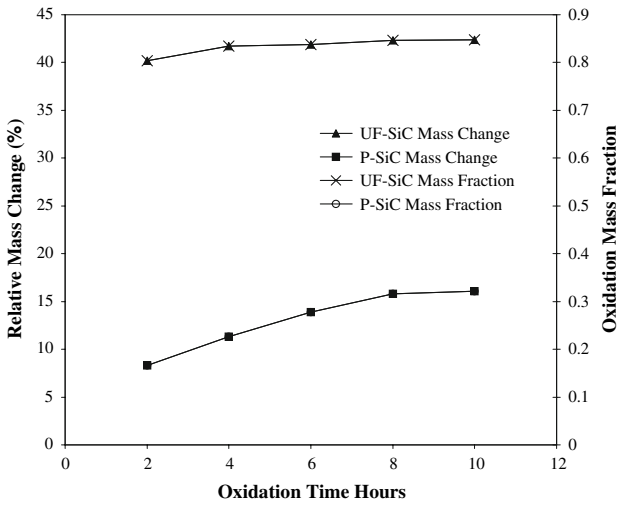

Fig. 4 Relative mass change and mass fraction oxidized against oxidation time (at 1,200 °C)

occurring simultaneously with the oxidation reaction at high temperature, which hinders the further oxidation of SiC [10], and/or to a change in the oxidation mechanism and/or kinetics (which could occur in both the loose powder and the SiC-containing nanocomposite).

Figures 5 and 6 show the relative mass change and mass fraction oxidized versus holding time at different temperatures in static air for UF-SiC and P-SiC, respectively. It can be observed that at 1,000 and 1,100 °C, the relative mass change and oxidation mass fraction increase with time for both UF-SiC and P-SiC. At 1,200 °C, this is not the case for either SiC powder; for UF-SiC, after 4 h holding time, no further mass and oxidation mass fraction increase was observed, while for P-SiC, after about 8 h holding time, the rate of mass change, i.e., degree of

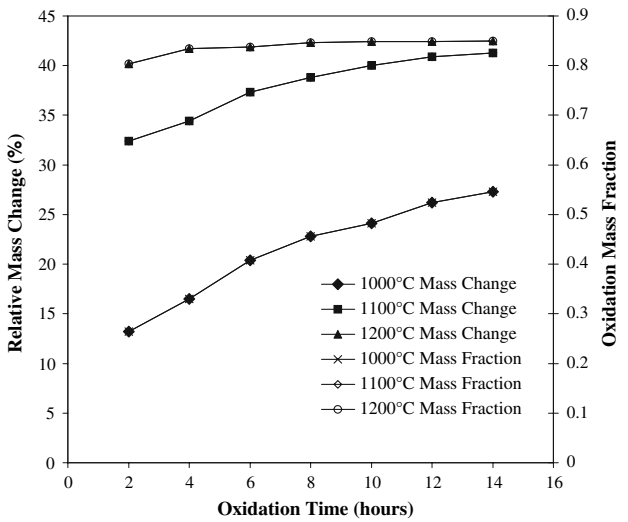

Fig. 5 Relative mass change and oxidation mass fraction of UF-SiC against oxidation time

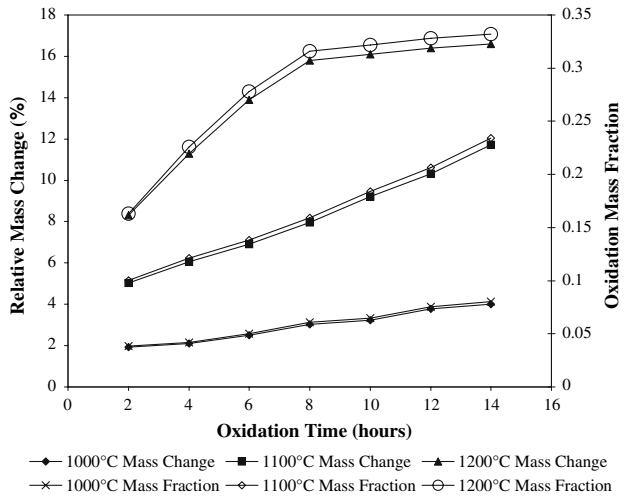

Fig. 6 Relative mass change and oxidation mass fraction of P-SiC against oxidation time

oxidation, decreased noticeably, producing a change in slope. This means that the oxidation processes of both UF-SiC and P-SiC experienced some change at 1,200 °C.

Figures 7 and 8 show the X-ray diffraction (XRD) patterns for the P-SiC powder and the UF-SiC powder before and after oxidation at different temperatures for different times, respectively. The XRD patterns revealed an obvious decrease in the amount of SiC and a corresponding increase in the amount of SiO_2 as the oxidation temperature increased. For P-SiC, at 1,200 °C (after 10 h oxidation) and above, the SiO_2 formed is cristobalite. For UF-SiC, below about 1,200 °C, the broad peak around 22.9° 2θ indicates that the SiO_2 is amorphous. As the oxidation temperature increased, the peak narrowed, becoming more intense. After about 4 h at 1,200 °C, the peaks corresponding to cristobalite could be detected. Since the presence of amorphous silica will accelerate the later sintering of the composite, oxidation of the SiC below 1,200 °C is preferable.

For the isothermal oxidation of powders, Carter's equation [11] is followed:

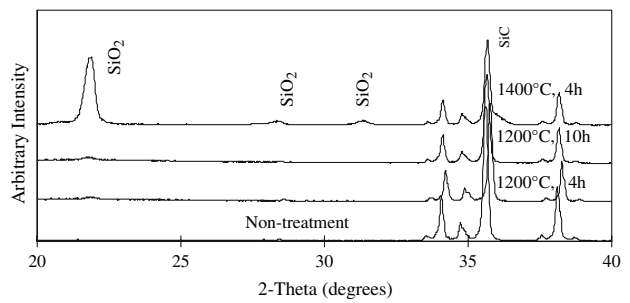

Fig. 7 X-ray diffraction pattern for P-SiC before and after oxidation under different conditions

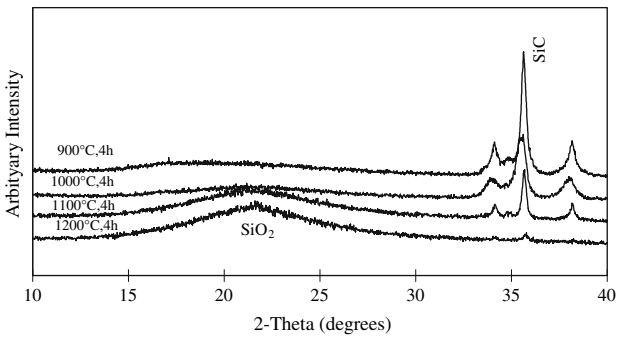

Fig. 8 X-ray diffraction pattern for UF-SiC after oxidation under different conditions

$$z-(z-1)(1-f)^{\frac{2}{3}}-[1+(z-1)f]^{\frac{2}{3}}=\frac{2(z-1)k}{r^2}t=K't \tag{2}$$

where f is the degree of reaction (i.e., the oxidation fraction of SiC after time t), r is the particle radius of the initial powder, z is the ratio of the molar volume of the product to the molar volume of the reactant (for the oxidation of SiC to amorphous SiO_2 $z=(M_{SiO_2}/\rho_{SiO_2})/(M_{SiC}/\rho_{SiC})=(60.09/2.2)/(40.1/3.21)=2.186$) and k and K' are the rate constants. Hence, the rate constant K' at each temperature could be obtained from the slope of the fitted line to a plot of $C=z-(z-1)(1-f)^{\frac{2}{3}}-[1+(z-1)f]^{\frac{2}{3}}$ versus time t. Apparently, C is a reaction function that can represent the degree of the reaction from SiC to SiO_2.

The plots of $C=z-(z-1)(1-f)^{\frac{2}{3}}-[1+(z-1)f]^{\frac{2}{3}}$ versus oxidation time t for the UF-SiC and P-SiC powders are shown in Figs. 9 and 10, respectively. Generally, $C=z-(z-1)(1-f)^{\frac{2}{3}}-[1+(z-1)f]^{\frac{2}{3}}$ varied linearly with the oxidation time when samples were oxidized at temperatures below 1,200 °C. At 1,200 °C, when UF-SiC and P-SiC powders were oxidized for more than 4 and 8 h, respectively, the data deviated from the linear relationship and exhibited lower mass gains than predicted by Carter's equation. The decrease in the mass gain fraction of the samples oxidized at 1,200 °C for long periods is associated with the structural change occurring at this temperature with time as proved by the XRD traces in Figs. 7 and 8. The formation of cristobalite in the oxidation layer has been shown to reduce the oxidation rate of SiC [4, 5, 12, 13].

The rate constants K' of UF-SiC and P-SiC were calculated from the slopes of each fitting line in Figs. 9 and 10 and are listed in Table 1. The Arrhenius plots of rate constant K' versus oxidation temperature for UF-SiC and P-SiC are shown in Figs. 11 and 12, respectively. From the slope of each line, the activation energies of the oxidation were calculated to be 51.0 and 281.1 kJ/mol for UF-SiC and P-SiC, respectively. (slope = −activation energy/gas

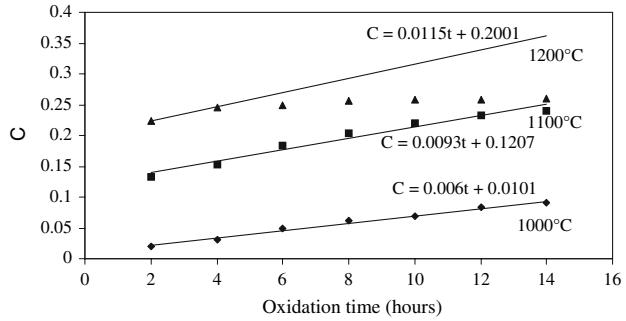

Fig. 9 Relationship between reaction function C and oxidation time for UF-SiC

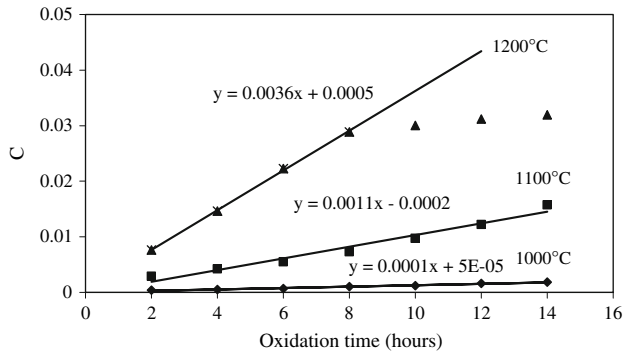

Fig. 10 Relationship between reaction function C and oxidation time for P-SiC

Table 1 Rate constant K' as function of oxidation temperature for UF-SiC and P-SiC

Temperature (°C)	Rate constant of UF-SiC (h^{-1})	Rate constant of P-SiC (h^{-1})
1,000	0.006	0.0001
1,100	0.0093	0.0011
1,200	0.0115	0.0036

constant). The activation energy of UF-SiC is much smaller than P-SiC owing to its very fine nature.

The activation energies quoted in the literature for SiC oxidation are quite inconsistent; varying, not unexpectedly,

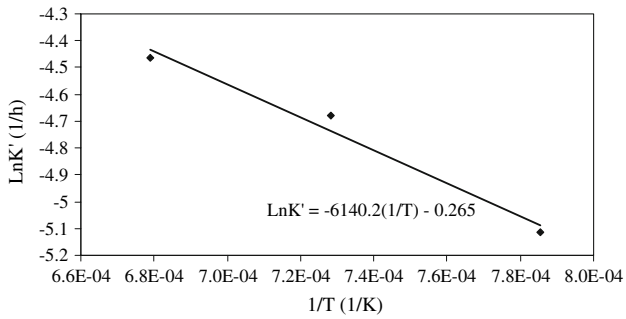

Fig. 11 Arrhenius plot of oxidation rate constant K' versus oxidation temperature for UF-SiC

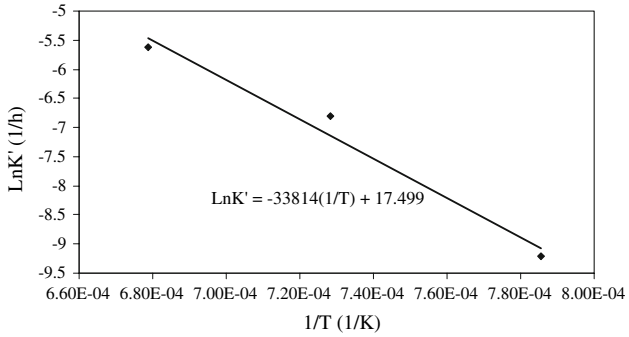

Fig. 12 Arrhenius plot of oxidation rate constant K' versus oxidation temperature for P-SiC

with the sample nature, e.g., bulk, film or powder; single crystal, or polycrystals [3, 7, 13–15]. Nevertheless, the proposed mechanisms for the oxidation of SiC are quite consistent. The oxidation mechanisms are believed to be the permeation of molecular oxygen at lower temperatures (<1,350 °C) and the diffusion of oxygen ions at higher temperatures (>1,350 °C).

Since the oxidation of SiC is an oxygen consuming process, as the partial pressure of oxygen increases, the driving potential for the reaction increases, and hence, so does the extent of oxidation. Figure 13 compares the oxidation behaviour of UF-SiC in static air and flowing air (at a flow rate of 30 cm^3/min). As expected, under the same temperature and time conditions, the oxidation mass fraction in flowing air is higher than that in static air.

A recent study [16] of the oxidation (apparently in static air) of SiC loose powder particles, in order to enable their incorporation in a borosilicate glass matrix, investigated

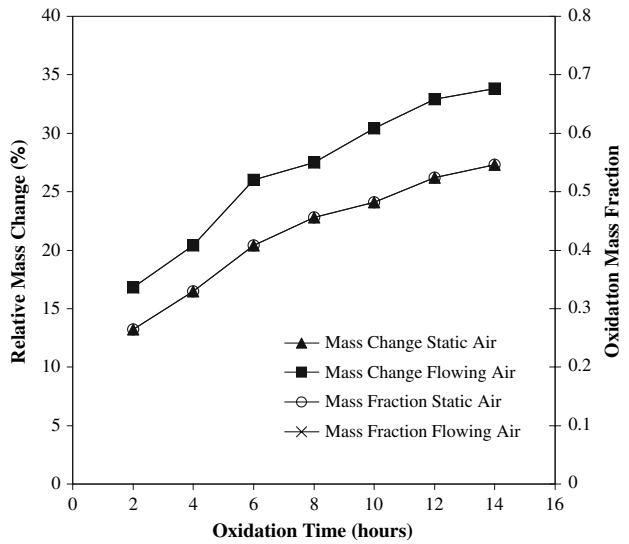

Fig. 13 Relative mass change and oxidation mass fraction of UF-SiC versus oxidation time (at 1,000 °C) in static air and flowing air

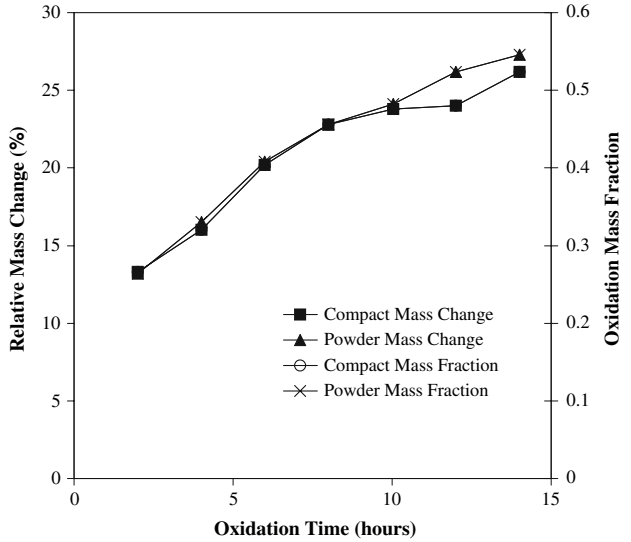

Fig. 14 Relative mass change and oxidation mass fraction of SiC as loose powder and in a BA_5/20 wt.% SiC compact versus oxidation time (at 1,000 °C)

the oxidation behaviour of SiC powders, with as-received average particle sizes ranging from 3.7 to 140.5 μm, at temperatures from 800 to 1,500 °C for 2 h, and also oxidized the 3.7 μm powder for times from 10 min to 48 h at 1,200 °C. The results of this study showed the Deal–Grove diffusion-reaction model [6] dependence of the 3.7 μm SiC powder oxidation kinetics and confirmed that the most efficient oxidation is achieved within the first 5 h of thermal treatment.

In order to understand the difference in the oxidation behaviour of SiC in loose powder form and when it is incorporated in pressure-filtered nanocomposite compacts, experiments to determine the oxidation behaviour of SiC in a pressure filtered BA_5/20 wt.% SiC compact were carried out. Figure 14 shows the relative mass change and

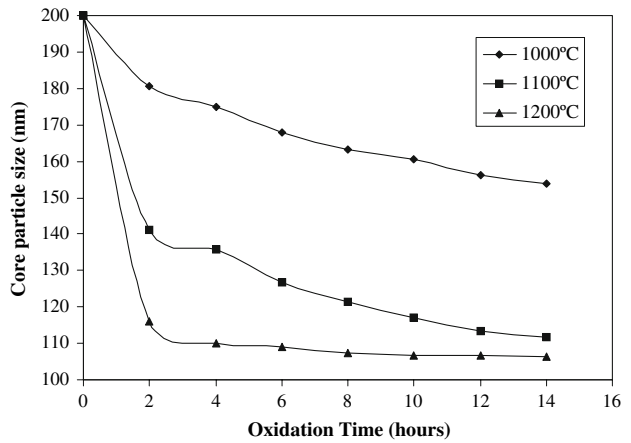

Fig. 15 The dependence of the calculated UF-SiC core particle size on oxidation time at different temperatures

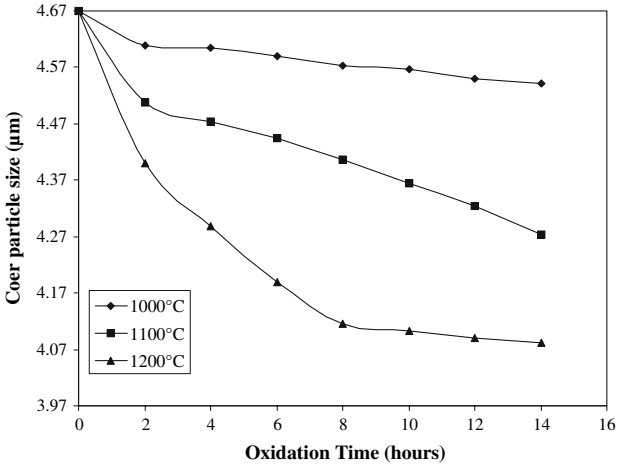

Fig. 16 The dependence of the calculated P-SiC core particle size on oxidation time at different temperatures

oxidation mass fraction of SiC in both loose powder and SiC-composite compact forms as a function of holding time (at 1,000 °C). Note that there is no apparent difference between the oxidation behaviour of the SiC as loose powder and when it is within the SiC-containing nanocomposite compact. This means that although the pressure-filtered compact has a high density, its pore size is still large enough for oxygen molecules to readily diffuse in. The high oxidation mass fraction of SiC in Al_2O_3–SiC and SiC/alumina/zirconia compacts as reported by Sakka et al. [10], Kaya [17] and Lin [5], supports this view.

Particle size analysis and microstructures

For simplicity, suppose that all of the SiC particles have the same size and all of them are spherical. If the radius of the initial SiC particle, the radius of the remnant SiC particle, the radius of the particle after oxidation and the thickness

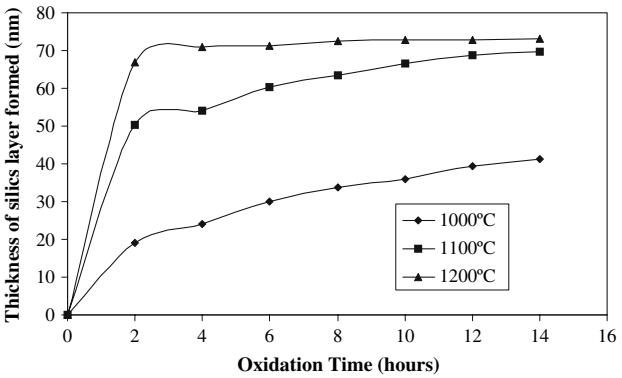

Fig. 17 The dependence of the thickness of the silica layer formed on UF-SiC particles on oxidation time at different temperatures

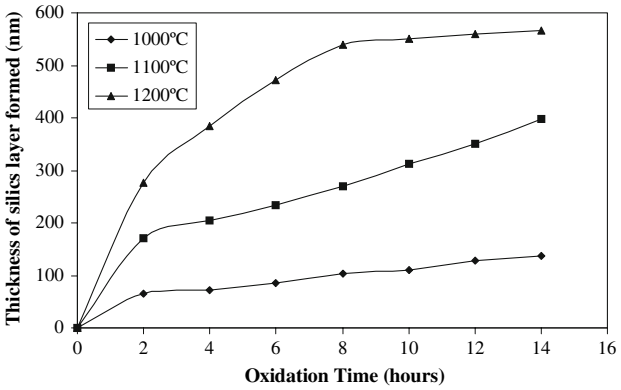

Fig. 18 The dependence of the thickness of the silica layer formed on P-SiC particles on oxidation time at different temperatures

of the SiO_2 formed are expressed by r_1, r_2, r_3 and Δr, respectively, the following relationships (derived in Appendix B) stand:

$$r_2 = r_1\sqrt[3]{1-f} \tag{3}$$

$$r_3 = r_1\sqrt[3]{1+f(z-1)} = r_1\sqrt[3]{1+1.186f} \tag{4}$$

$$\Delta r = r_3 - r_2 = r_1\left[\sqrt[3]{1+f(z-1)} - \sqrt[3]{1-f}\right] = r_1\left[\sqrt[3]{1+1.186f} - \sqrt[3]{1-f}\right] \tag{5}$$

So by controlling the oxidation mass fraction of SiC, that is by controlling the oxidation temperature and time, the expected SiC core particle size ($2r_2$), the particle size of the whole particle after oxidation ($2r_3$) and the thickness of SiO_2 formed ($\Delta r = r_3 - r_2$) can be obtained. The initial mean particle sizes of UF-SiC and P-SiC are 200 nm ($r_1 = 100$ nm) and 4.7 μm ($r_1 = 2.35\,\mu$m), respectively. From Eqs. 3, 4 and 5, after partial oxidation, the SiC core particle size ($2r_2$), the particle size of the whole particle after oxidation ($2r_3$) and the thickness of SiO_2 formed ($\Delta r = r_3 - r_2$) can be calculated.

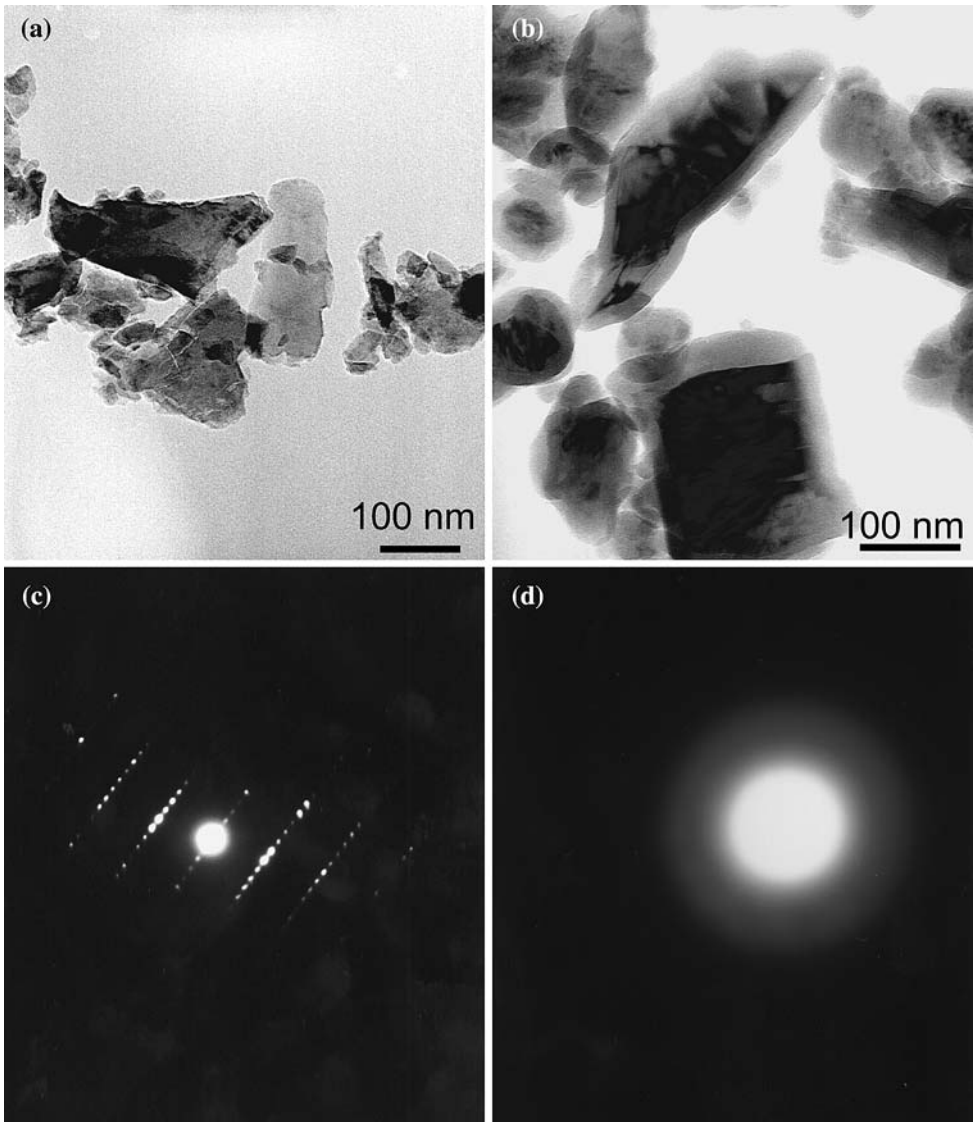

Fig. 19 TEM micrographs of UF-SiC powder (**a**) before and (**b**) after oxidation at 1,000 °C for 4 h, and the TEM electron diffraction pattern of (**c**) a UF-SiC core particle and (**d**) the SiO_2 layer surrounding the UF-SiC core particle

Figures 15 and 16 show the effect of holding time (at different temperatures) on the calculated SiC core particle for UF-SiC and P-SiC, respectively. Figures 17 and 18 show the effect of holding time (at different temperatures) on the calculated thickness of the SiO_2 surface layer formed on the UF-SiC and P-SiC particles, respectively. As expected the SiC core particle size decreases with increasing oxidation time and/or temperature, with the thickness of the SiO_2 surface layer increasing simultaneously.

Figure 19a and b shows TEM micrographs of the UF-SiC powder before and after oxidation at 1,000 °C for 4 h, respectively. It is clear that after oxidation, the SiC particles are surrounded by a layer of silica. In the bottom middle of Fig. 19b, there is a tabular UF-SiC particle with a particle size between 150 and 200 nm, whose silica layer is about 25 nm in thickness, which correlates well with the calculated result of 24 nm after oxidation at 1,000 °C for 4 h; see Fig. 17. The difference originates from the assumption made in the calculation, that all the particles are spherical with a diameter of 200 nm. As Fig. 19a shows, this is clearly not the case, since the particles are not spherical and vary in size; thus, the remnant SiC core particle size, the size of the whole core-shell particle after oxidation, and the thickness of the encapsulating SiO_2 surface layer or shell will differ according to the initial pre-oxidized SiC particle morphology and size.

In order to simply illustrate the nature of the post-oxidation SiC core-SiO_2 shell structure of the oxidized particles, Fig. 19c is the selected area diffraction (SAD) pattern of a core particle, like the particles seen in Fig. 19b with an encapsulating layer of silica, confirming it to be crystalline SiC. By way of contrast, Fig. 19d gives the CBED pattern of the surrounding silica surface layer of the same particle, showing that the silica formed at 1,000 °C for 4 h is amorphous, as confirmed by the XRD trace in Fig. 8.

Figure 20 shows the differential number particle size distribution of P-SiC before and after oxidation at 1,200 °C for 4 h, while Fig. 21 shows the corresponding differential volume particle size distribution of UF-SiC before and after oxidation at 1,200 °C for 4 h.

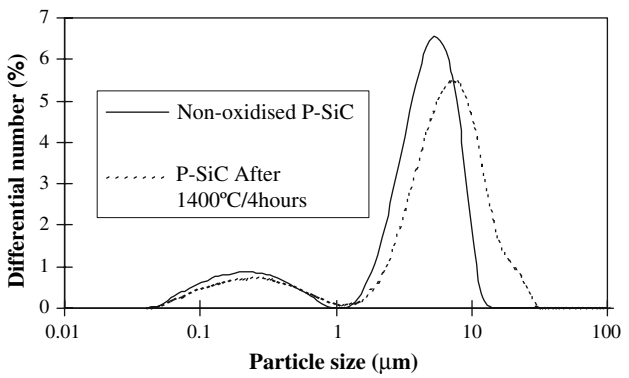

Fig. 20 Particle size distribution of P-SiC before and after oxidation (1,200 °C/4 h)

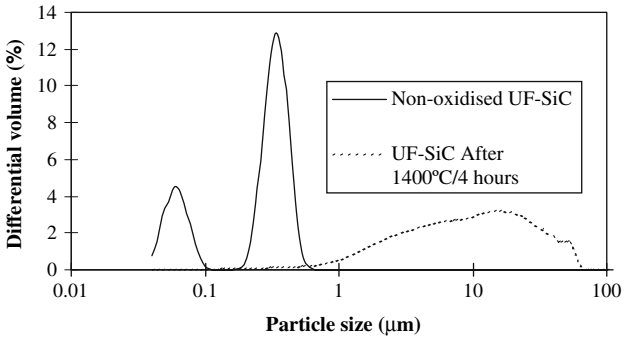

Fig. 21 Particle size distribution of UF-SiC before and after oxidation (1,200 °C/4 h)

Particle size analysis shows that after oxidation, the particle size distributions of both SiC particle types shift to a larger particle size. This is in accordance with what is predicted since the oxidation of SiC is a mass-gain process

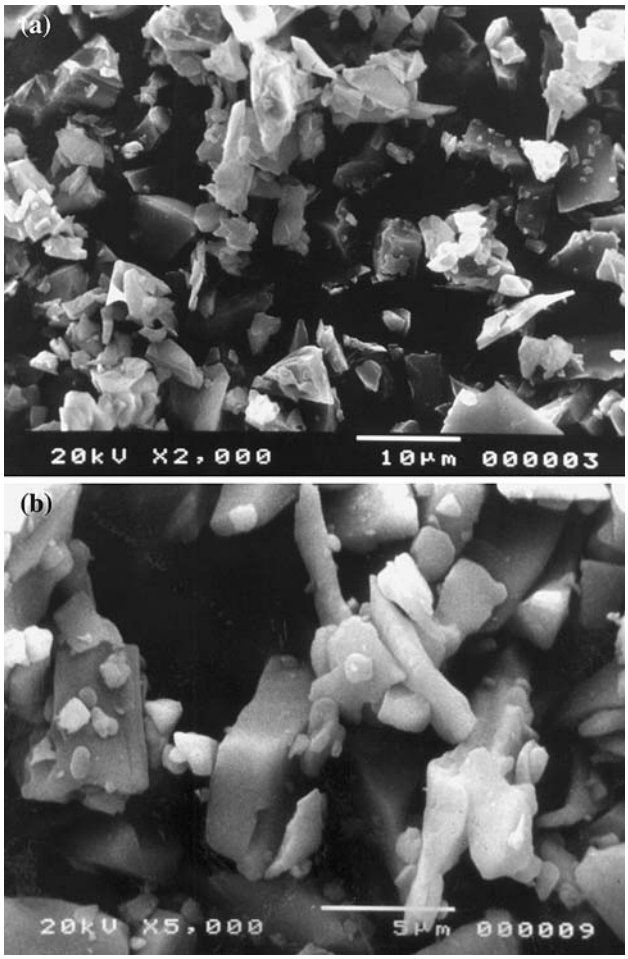

Fig. 22 SEM micrographs of P-SiC; (**a**) raw powder, (**b**) after 1,200 °C/4 h oxidation

and the density of SiO_2 (cristobalite 2.65 g cm^{-3} and amorphous SiO_2 2.22 g cm^{-3}) is smaller than that of SiC (3.2 g cm^{-3}). However, the marked increase in the UF-SiC particle size after oxidation cannot be explained in terms of oxidation mass and volume gain alone. Possible explanations are the sintering of the powder at high temperature; agglomeration of the oxidized powder which derives from the agglomeration of the raw UF-SiC powder due to its small particle size and hence high surface area to volume ratio. Thus, a low oxidation temperature is desirable in order to obtain a fine particle size. Figures 22 and 23 show secondary electron imaging SEM micrographs of the P-SiC and UF-SiC powders, respectively, before and after oxidation (1,200 °C, 4 h). In the case of P-SiC, Fig. 22 shows that after oxidation, the edges of the oxidized particles are not as sharp as those of the original SiC particles, whereas for UF-SiC after oxidation, extensive agglomeration, as indicated by the particle size analysis, is confirmed by Fig. 23.

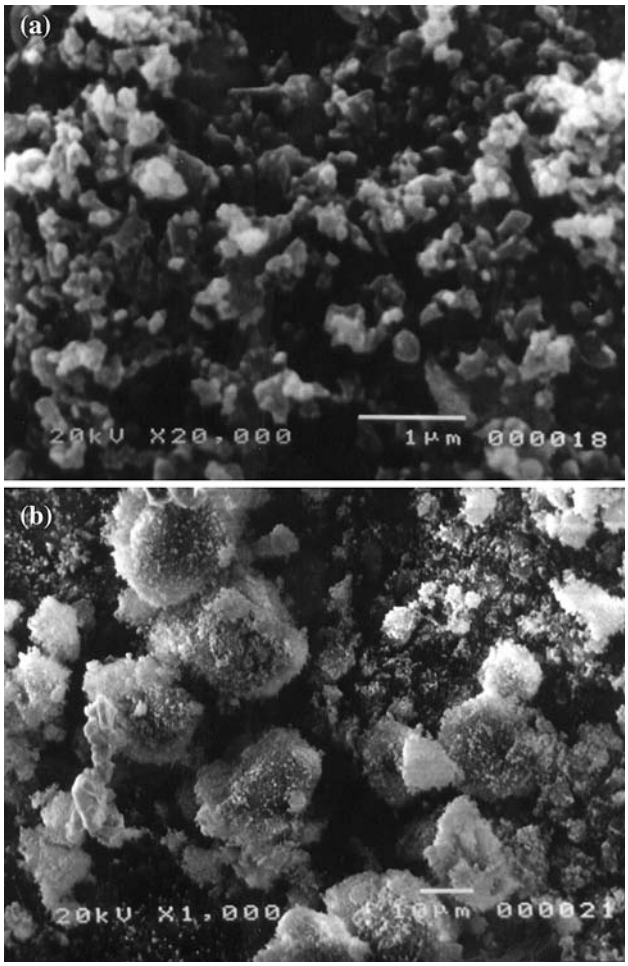

Fig. 23 SEM micrographs of UF-SiC; (**a**) raw powder, (**b**) after 1,200 °C/4 h oxidation

Conclusions

The oxidation behaviour, in static air and flowing air, of a submicron size SiC powder and a micron size SiC powder, each with a differing particle size and morphology distribution, has been investigated, in both loose powder form and incorporated in pressure-filtered SiC/mullite/alumina nanocomposite compacts. Furthermore, the effect of temperature and time on the mass fraction of SiC oxidized, the nature of the particle size, particle morphology and agglomeration behaviour pre- and post-oxidation has been discussed.

The TGA–DTA analysis and the oxidation studies both indicate that the onset of significant oxidation occurs at a much lower temperature for UF-SiC than for P-SiC due to the particle size of UF-SiC being much smaller than that of P-SiC. Consequently, under the same oxidation conditions, the rate and extent of oxidation of UF-SiC is much higher than that of P-SiC.

When SiC powder is used to prepare SiC/mullite/alumina nanocomposites, a SiC particle down to nanometer size after oxidation is desired. It is invariably necessary that the extent of the oxidation is controllable in order to achieve the desired core SiC size and SiO_2 surface layer thickness, to thereby control both the SiC particle size (and hence the amount of SiC) and the amount of silica (and hence mullite) in the nanocomposites. The oxidation results show that SiC core particles down to nanometre size could not be formed in the P-SiC (micron particle size) powder after oxidation at 1,400 °C for 10 h, and that the extent of oxidation is low. In the case of the UF-SiC (submicron particle size) powder, the oxidation behaviour was both more controllable and efficient in terms of the extent of oxidation and hence the remnant SiC core particle size and the concomitant silica surface layer thickness. Thus, the UF-SiC powder proved suitable for the preparation of SiC/mullite/alumina nanocomposites where the core SiC particle size and amount of silica both need to be controlled for the purposes of SiC nanoparticle incorporation and mullite formation, respectively.

The XRD traces of the oxidized powder show that the SiO_2 layer formed is amorphous when SiC powder is oxidized below 1,200 °C but crystalline (as cristobalite) when oxidized above 1,200 °C, and so since the presence of amorphous silica can accelerate the sintering of the nanocomposite, the oxidation of SiC powder should take place below 1,200 °C. Owing to agglomeration of the oxidized SiC powder at high temperatures, oxidation at a lower temperature for a longer time is recommended provided the desired extent of oxidation can be achieved. Achieving a high degree of oxidation at relatively low temperatures without inordinately long oxidation times

being required is aided by the fact that the oxidation mass fraction in flowing air is higher than in static air.

Finally, this investigation of the oxidation behaviour of SiC powder particles indicates that there is no apparent difference between the oxidation behaviour of the SiC as loose powder and when it is within a SiC-containing pressure-filtered nanocomposite powder compact for the given pressure filtration conditions and starting materials. Thus, the SiC/mullite/alumina nanocomposite composition could be confidently predicted using the SiC loose powder oxidation data and behaviour.

Acknowledgements The work presented here is a part of Jingyan He's PhD research undertaken in the Department of Metallurgy and Materials and the IRC in Materials Processing at the University of Birmingham, under the supervision of C. B. Ponton. Thus, the authors are grateful to the Department/IRC for the provision of laboratory facilities and to all the technical and academic staff therein for the help extended to Jingyan during his PhD. This work would not have been initiated by C. B. Ponton, had his own enthusiasm for materials science not been encouraged and nurtured in the direction of ceramic materials by Professor Rees Rawlings, first via undergraduate lectures and labs, then during a final-year undergraduate project that was followed by a PhD on CMAS glass-ceramics (both supervised by Rees Rawlings and Dr Philip Rogers), culminating in his doing post-doctoral research on bioactive apatite-containing glass-ceramics with Rees, after which he obtained an academic post in the IRC in Materials Processing/Department of Metallurgy and Materials at the University of Birmingham.

Appendix A: calculation of the relative weight gain and oxidation mass fraction of SiC particles in SiC powders

If the oxidation behaviour of SiC is in accordance with the following oxidation reaction [2]:

$$\underset{\substack{40.1\\X}}{SiC} + 2O_2 \rightarrow \underset{\substack{60.09\\Y}}{SiO_2 + CO_2}$$

$$Y = \frac{M_{SiO_2}}{M_{SiC}}X = \frac{60.09X}{40.1} = 1.50X \tag{A1}$$

where X is the mass of SiC which has been oxidized, Y is the corresponding mass of SiO_2 formed;M_{SiO_2} and M_{SiC} are the molecular masses of SiO_2 and SiC, respectively.

Assuming the mass of the sample before and after oxidation is M_S and M'_S, respectively, thus,

$$\frac{Y - X}{M_S} = \frac{M'_S - M_S}{M_S} = C_M \tag{A2}$$

where C_M is the relative mass change after oxidation. Substituting Eqs. A1 into A2 gives:

$$C_M = \frac{1.50X - X}{M_S} \therefore \frac{X}{M_S} = \frac{C_M}{0.5}, \tag{A3}$$

In fact X/M_S is the oxidation fraction of SiC. If we use f to express it, thus

$$f = \frac{C_M}{0.5} = 2C_M \tag{A4}$$

Appendix B: theoretical derivation of the size change of a SiC particle after oxidation

Since the oxidation of SiC is a mass-gain process and the density of amorphous SiO_2 ($\rho_{SiO_2} = 2.2\,g\,cm^{-3}$) is less than that of SiC ($\rho_{SiC} = 3.21\,g\,cm^{-3}$), the particle size will be increased after oxidation. Supposing that all of the SiC particles have the same size and all of them are spherical, this process can be shown in Fig. B1.

Here r_1 is the radius of the initial SiC particle, r_2 is the radius of the remaining SiC particle, r_3 is the radius of the particle after oxidation and $r_3 - r_2 = \Delta r$ is the thickness of the SiO_2 formed.

Thus, the initial mass of a SiC particle, M, is $\frac{4}{3}\pi r_1^3\rho_{SiC}$, and after oxidation, its mass is $\frac{4}{3}\pi r_2^3\rho_{SiC}$. Thus, the mass of oxidized SiC, X, is:

$$\frac{4}{3}\pi r_1^3\rho_{SiC} - \frac{4}{3}\pi r_2^3\rho_{SiC} \tag{B1}$$

So the oxidation mass fraction is:

$$f = \frac{\frac{4}{3}\pi r_1^3\rho_{SiC} - \frac{4}{3}\pi r_2^3\rho_{SiC}}{\frac{4}{3}\pi r_1^3\rho_{SiC}} \tag{B2}$$

$$\therefore r_2 = r_1\sqrt[3]{1-f} \tag{B3}$$

From Eq. B1, the mass of SiO_2 formed, Y, is:

$$Y = \left(\frac{4}{3}\pi r_3^3 - \frac{4}{3}\pi r_2^3\right)\rho_{SiO_2} \tag{B4}$$

According to Eq. A1 in Appendix A

$$Y = \frac{M_{SiO_2}}{M_{SiC}}X = \frac{60.09X}{40.1} = 1.50X$$

Substituting Eqs. B1 and B4 into Eq. A1 above gives:

$$r_3^3 = r_2^3 + \left(r_1^3 - r_2^3\right)z \tag{B5}$$

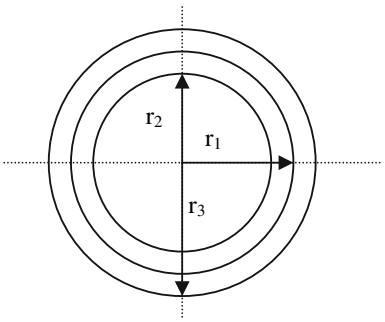

Fig. B1 The schematic diagram of the change of SiC particle after oxidation

where $z = \left(\frac{M_{SiO_2}}{\rho_{SiO_2}}\right)/\left(\frac{M_{SiC}}{\rho_{SiC}}\right) = \left(\frac{60.09}{2.2}\right)/\left(\frac{40.1}{3.21}\right) = 2.186$ is the ratio of the molar volume of SiO_2 to that of SiC.

Substituting equation B3 into B5 gives:

$$r_3 = r_1\sqrt[3]{1+f(z-1)} = r_1\sqrt[3]{1+1.186f} \quad \text{(B6)}$$

Thus, the thickness of the SiO_2 formed, $\Delta r = r_3 - r_2$, is:

$$\Delta r = r_3 - r_2 = r_1\left[\sqrt[3]{1+f(z-1)} - \sqrt[3]{1-f}\right] = r_1\left[\sqrt[3]{1+1.186f} - \sqrt[3]{1-f}\right] \quad \text{(B7)}$$

References

1. Shi Z, Lee J, Zhang D, Lee H, Gu M, Wu R (2001) J Mater Tech 110:127
2. Vaughn WL, Maahs HG (1990) J Am Ceram Soc 73(6):1540
3. Ramberg CE, Cruciani G, Spear KE, Tressler RE, Ramberg CF Jr (1996) J Am Ceram Soc 79(3):730
4. Ogbuji LUJT (1997) J Am Ceram Soc 80(6):1544
5. Lin YJ, Chen LJ (2000) Ceram Int 26:593
6. Deal BE, Grove AS (1965) J Appl Phys 36(12):3770
7. Opila EJ (1994) J Am Ceram Soc 77(3):730
8. Holz D, Claussen N (1995) Ceram Eng Sci Proc 16(1):252
9. Wu S, Claussen N (1994) J Am Ceram Soc 77(11):2898
10. Sakka Y, Bidinger DD, Aksay IA (1995) J Am Ceram Soc 78(2):479
11. Carter RE (1961) J Chem Phys 34:2010
12. Liu DM (1997) Ceram Int 23:425
13. Costello JA, Tressler RE (1986) J Am Ceram Soc 69(9):674
14. Singhal SC (1976) J Mater Soc 29:1246
15. Pultz WW (1967) J Phys Chem 71(13):4556
16. Villegas M, Sierra T, Lucas F, Fernández JF, Caballero AC (2007) J Euro Cer Soc 27:861–865
17. Kaya C (1999) PhD thesis, University of Birmingham